THE BELL SYSTEM TECHNICAL JOURNAL
Vol. 62, No. 2, February 1983
Printed in U.S.A.

An Analysis of the Derivative Weight-Gain Signal From Measured Crystal Shape: Implications for Diameter Control of GaAs

By A. S. JORDAN, R. CARUSO, and A. R. VON NEIDA

(Manuscript received May 11, 1982)

A commercially viable GaAs device technology for field-effect transistors, integrated circuits, and lasers is critically dependent on the availability of high-quality, single-crystal boules with controlled diameter. We have modeled a diameter control scheme based on the monitoring of crystal weight for liquid-encapsulated Czochralski (LEC) growth of GaAs. The presence of the B_2O_3 liquid encapsulant and significant capillary forces make the direct interpretation of the weight-gain signal and its time derivative (DWGS) more complicated in comparison with pulled materials such as oxide crystals. We have formulated a realistic model for the LEC growth of axisymmetric crystals and have derived the differential equation relating the time evolution of the DWGS to radius and length. We show that the magnitude of the DWGS at the crystal's "shoulder" is inversely related to the radius of curvature. Furthermore, the meniscus by itself gives rise to a precursor or early warning in the signal, which means that the maximum in DWGS precedes the maximum in shape by a few hundred seconds. The existence of a secondary maximum or aftershock in the signal that is the sole consequence of liquid encapsulation is also demonstrated. Excellent agreement has been obtained between DWGS and the signal predicted from the measured shape of a grown crystal. Thus, prospects for automatic diameter control are encouraging.

I. INTRODUCTION

GaAs is one of the key semiconductor materials that serves as a substrate for light-emitting diodes (LEDs), lasers, and field-effect transistors (FETs). Paralleling the development pattern of growth techniques for other single crystals, the issues of primary interest have

evolved from questions of quality (elimination of twinning and defects, doping uniformity) to that of economy of size. However, scaling up the dimensions of GaAs crystals grown by the liquid-encapsulated Czochralski (LEC) technique necessitates introducing sophisticated schemes for diameter control. By achieving satisfactory control, it will also be possible to run for extended periods of time with minimal supervision, and to attain higher crystal yields, as well as a reduction in defect generation brought on by shape change.

Since diameter control in Czochralski growth has been the subject of an excellent recent review by Hurle,[1] here a brief outline of previous efforts with respect to LEC growth will suffice. Unlike Si[2] and a wide variety of oxide crystals[3] (e.g., GGG, $LiTaO_3$) for which successful diameter measurement and control systems have been developed, the realization of a viable system for the LEC growth of III-V compounds has been much more difficult to achieve. This is largely due to effects associated with the growth chamber under high pressure, the presence of the encapsulating layer of $B_2O_3(\ell)$, and the phenomenon of anomalous density ($d_{liquid} > d_{solid}$) in some semiconductor materials.

A number of approaches to the control problem have been taken. Pruett and Lien,[4] and van Dijk et al.[5] have employed an X-ray beam passing through the high-pressure growth apparatus for GaP, designed to make the melt a high absorber of radiation relative to all other materials in the radiative path of the system. The subsequent use of an image intensifier gave an accurate television picture of the growth interface. Small changes in diameter could then be electronically extracted from the video signal and utilized for its control.[5]

Alternatively, considerable success has been achieved meeting the demand for large, closely controlled diameter GaP single crystals using a floating die technique. Cole et al.[6] employed a Si_3N_4 ring floating in the GaP melt beneath the $B_2O_3(\ell)$. This modified form of Stepanov ring[6,7] creates a long-term stable growth regime, permitting diameter tolerances of ±1 mm for a 50-mm diameter boule. The technique has also been applied to GaAs with different degrees of success, apparently depending on the crystallographic growth direction.[8]

In a third technique, advocated by Bardsley et al.,[9] a weight signal or a derivative weight-gain signal obtained by detecting the apparent weight change of either the crucible or crystal during Czochralski growth is used to control the power output and consequently the diameter. Bardsley et al. have considered both the theory[9] and its implementation by an analogue servo-system.[10] Although these authors have proposed reasonable initial postulates and expressions to calculate the weight gain, the detailed analysis is limited only to small perturbations in diameter and the formalism precludes growth by the LEC technique.

For some time now we have routinely measured the apparent weight of LEC-pulled GaAs crystals with a high sensitivity load cell placed in the high-pressure chamber in series with the crystal pull rod. The output of the cell is recorded as a dc level. Then, the derivative of the signal is taken electronically with a device developed especially for that purpose, and is also recorded. This activity has served as a useful qualitative guide in the manual control of diameter. The major objective of this paper is to develop the fundamental theory that governs the relationship between the shape of an axisymmetric crystal with arbitrary variations in its diameter (including the shoulder) grown by the LEC technique and the instantaneously detected derivative weight-gain signal. Besides gaining new physical insight, we expect that by means of these investigations we can focus on the important physical factors and analytical techniques essential to the eventual control of crystal diameter.

As a first step, a tractable model is formulated for LEC growth with a meniscus. The treatment leads to an explicit expression for the derivative weight-gain signal exclusively in terms of the crystal cross section and its first and second derivatives, in addition to geometrical and material parameters. Next, the numerical techniques required to perform computer simulations are outlined. Then, the key features of the signal are investigated by using the probability density function of the lognormal distribution for the crystal contour. Among the effects considered in detail are the shape of the shoulder and the presence or absence of the $B_2O_3(\ell)$ encapsulant and meniscus. Furthermore, the derivative weight-gain signal is predicted for four contour lines—generated by consecutive 90° axial rotations—of a specially prepared GaAs boule and compared with the signal measured during growth. Finally, in light of these modeling calculations, the prospective techniques for diameter control are discussed.

II. THEORY

In this section, by a consideration of the relevant features of the LEC growth process, a realistic model is developed for the derivative weight-gain signal in a form suitable for computer analysis. To make the calculations tractable, but without a serious loss of generality, the following set of assumptions and constraints has been introduced:

(*i*) The crystal and crucible are axisymmetric with circular cross sections. Hence, the crystal's radius, r, can always be prescribed as a function of the axial location, L, which is monotonically related to the time elapsed since seeding.

(*ii*) The crucible containing the melt and the encapsulant is a right circular cylinder of radius, R. Less restrictively, departures from

a right cylinder are permitted below the liquid level prevailing at the completion of growth.

(*iii*) The effects of crucible and crystal rotation and the concomitant viscous drag are neglected.

(*iv*) As the initial melt level falls by distance ℓ (Fig. 1), the entire amount of the liquid is transferred to the solid.

(*v*) Seepage from the $B_2O_3(\ell)$ encapsulating column of mass, m_B, and volume, V_B, to the melt/crucible interface (walls) is minute.

(*vi*) The solid-liquid interface is planar. This allows the separation of the associated heat transfer problem from the calculations.

(*vii*) Capillary forces between the melt, $B_2O_3(\ell)$, and solid result in a meniscus of height, h, with a subtended angle between the vertical

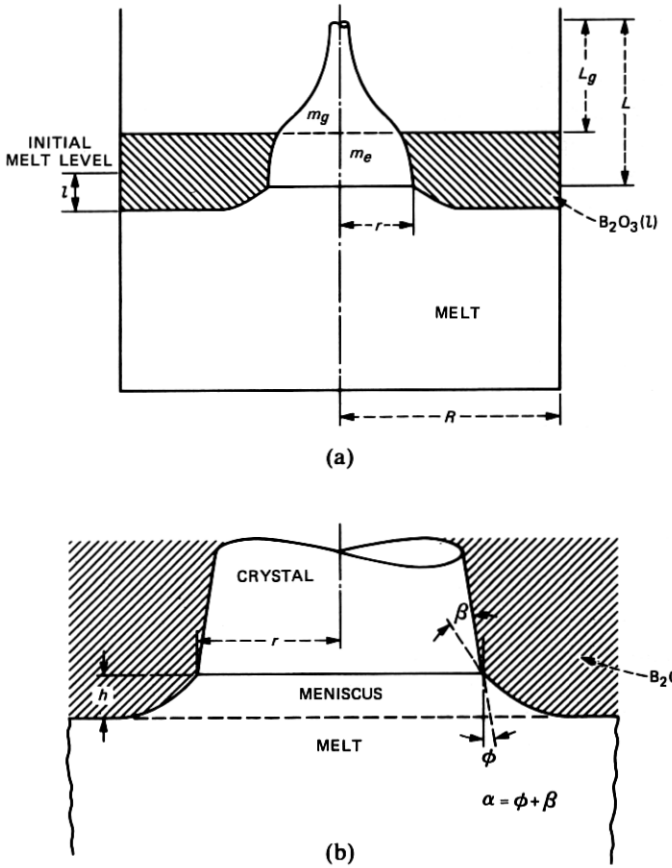

Fig. 1—(a) Schematic geometry of LEC pulling. (b) Enlarged view of the solid-liquid interface region.

and the tangent to the "skirt" of the meniscus (joining angle), α (Fig. 1).

(*viii*) As the crystal is pulled at constant rate p, contact with the melt is uninterrupted.

(*ix*) Physical constants required in the calculations are average values representative near the melting point of the crystal.

The preceding conditions in combination with the geometrical description of LEC pulling in Fig. 1 and Archimedes' principle permit writing the weight signal, W_s, corresponding to detected crystal mass, m_s, as the sum

$$W_s = m_s g = \underset{\substack{W_1 \\ \text{true weight}}}{} \quad \underset{\substack{-W_2 \\ \text{buoyancy correction to } W_1}}{} \quad \underset{\substack{+W_3 \\ \text{vertical projection of capillary force}}}{} \quad \underset{\substack{+W_4 \\ \text{weight of the cylindrical meniscus}}}{} \quad \underset{\substack{-W_5 \\ \text{buoyancy correction to } W_3 + W_4}}{} \tag{1}$$

where

$$W_1 = (m_e + m_g)g = mg \tag{2a}$$

$$W_2 = V_e \rho_B g \tag{2b}$$

$$W_3 = 2\pi r \sigma \cos \alpha \tag{2c}$$

$$W_4 = r^2 \pi h \rho_\ell g \tag{2d}$$

$$W_5 = V_{\text{men}} \rho_B g \tag{2e}$$

The symbols m, V, and ρ without subscripts designate the mass, volume, and density of the growing crystal, respectively. The same letters with subscripts B, ℓ, e, and g refer to the B_2O_3 encapsulant, melt, and that portion of the crystal that resides either in the encapsulant or the gas phase, respectively. The symbols σ and V_{men} represent the surface tension and meniscus volume, respectively.

Since $V_e = (m - m_g)/\rho$, with the abbreviation $k_1 = \rho_B/\rho$, $W_1 - W_2$ in eqs. (2a) and (2b) can be transformed into

$$W_1 - W_2 = m(1 - k_1)g + k_1 m_g g. \tag{3}$$

Then, differentiating eqs. (3), (2c), (2d), and 2e with respect to time, t, and using eq. (1), we obtain the derivative weight-gain signal (DWGS) in the form

$$\frac{dW_s/g}{dt} = (1 - k_1)\frac{dm}{dt} + k_1 \frac{dm_g}{dt} + \frac{2\pi}{g}\sigma \cos \alpha \frac{dr}{dt} - \frac{2\pi\sigma}{g} r \sin \alpha \frac{d\alpha}{dt} + \rho_\ell \left(2r\pi h \frac{dr}{dt} + r^2 \pi \frac{dh}{dt}\right) - \rho_B \frac{dV_{\text{men}}}{dt}. \tag{4}$$

It can be readily shown that dm/dt is a function of the other

variables. Clearly, if the crystal is axisymmetric, one has

$$\frac{dm}{dt} = \rho\pi r^2 \frac{dL}{dt}. \tag{5}$$

Moreover, the continuity of growth provides the relation

$$L = \ell + pt - h, \tag{6}$$

or in derivative form

$$\frac{dL}{dt} = \frac{d\ell}{dt} + p - \frac{dh}{dt}. \tag{7}$$

In addition, the conservation of matter during crystallization as the liquid level falls leads to

$$m = \rho_\ell(\pi R^2 \ell - V_{\text{men}}) \tag{8}$$

or

$$\frac{dm}{dt} = \rho_\ell \left(\pi R^2 \frac{d\ell}{dt} - \frac{dV_{\text{men}}}{dt} \right). \tag{9}$$

A combination of eqs. (5), (7), and (9) permits the elimination of $d\ell/dt$; hence eq. (5) can be rewritten as

$$\frac{dm}{dt} = \rho\pi r^2 \frac{\left(\frac{k dV_{\text{men}}}{\pi\ dt} + pr^2 - r^2 \frac{dh}{dt} \right)}{\bar{R}^2 + p - \frac{dh}{dt}}, \tag{10}$$

where $k = \rho_\ell/\rho$ and $\bar{R}^2 = \mathrm{kR}^2 - \mathrm{r}^2$.

Substituting eq. (10) into eq. (4) for the DWGS yields after several algebraic operations

$$\begin{aligned} \frac{dW_s/g}{dt} = {} & k_1 \frac{dm_g}{dt} + \frac{p(1-k_1)\pi\rho_\ell r^2 R^2}{\bar{R}^2} - \frac{2\pi\sigma}{g} r \sin\alpha \frac{d\alpha}{dt} \\ & + \frac{dV_{\text{men}}}{dt} \left[(1-k_1)\rho_\ell \frac{r^2}{\bar{R}^2} - \rho_B \right] + r^2\pi \frac{dh}{dt} \rho_\ell \left[1 - (1-k_1)\frac{R^2}{\bar{R}^2} \right] \\ & + 2\pi \frac{dr}{dt} \left[rh\rho_\ell + \frac{\sigma}{g} \cos\alpha \right]. \end{aligned} \tag{11}$$

In essence, the general form of the DWGS is given by eq. (11). Since all the variables directly depend on L or indirectly through r on L, it is convenient to replace the derivatives d/dt by $d/dL \cdot dL/dt$. Accordingly, we have

$$\frac{dW_s/g}{dt} = k_1 \frac{dm_g}{dL}\frac{dL}{dt} + \frac{p(1-k_1)\pi\rho_\ell r^2 R^2}{\bar{R}^2} - \frac{2\pi\sigma}{g} r \sin\alpha \frac{d\alpha}{dL}\frac{dL}{dt}$$

$$+ \frac{dV_{\text{men}}}{dL}\frac{dL}{dt}\left[(1-k_1)\rho_\ell \frac{r^2}{\bar{R}^2} - \rho_B\right] + r^2\pi \frac{dh}{dL}\frac{dL}{dt}\rho_\ell\left[1-(1-k_1)\frac{R^2}{\bar{R}^2}\right]$$

$$+ 2\pi \frac{dr}{dL}\frac{dL}{dt}\left(rh\rho_\ell + \frac{\sigma}{g}\cos\alpha\right). \quad (12)$$

Equation (12) completely describes the DWGS once the few remaining unknown functions are evaluated. These are the axial derivative of the crystal mass outside the $B_2O_3(\ell)(dm_g/dL)$, the macroscopic growth rate (dL/dt), and the meniscus (h, dh/dL, V_{men}, and dV_{men}/dL) in terms of $r(L)$ and the required physical and geometrical constants. The crystal shape $r(L)$ we consider here as an input signal and the choice of different functional forms will be postponed to the next section.

2.1 Evaluation of dm_g/dL

From Fig. 1 we conclude that the total cylindrical volume occupied by the segment of the growing crystal in V_e, the encapsulant, and the meniscus are conserved. Thus we can write the integral relation

$$\int_0^L r^2\pi dL - \int_0^{L_g} r^2\pi dL + V_{\text{men}} + V_B = \pi R^2(L - L_g + h), \quad (13)$$

where the two integrals on the left-hand side are equal to

$$\int_{L_g}^{L} r^2(L)\pi dL.$$

Thus we can express m_g/ρ as

$$m_g/\rho = \int_0^{L_g} r^2\pi dL = \int_0^L r^2\pi dL + V_{\text{men}} + V_B - \pi R^2(L - L_g + h).$$

Differentiating the above equation with respect to L gives

$$\frac{dm_g/\rho}{dL} = r^2\pi + \frac{dV_{\text{men}}}{dL} - \pi R^2\left(1 + \frac{dh}{dL} - \frac{dL_g}{dL}\right). \quad (14)$$

To obtain dL_g/dL we define a function $\phi(L, L_g) = 0$ by subtracting the right-hand side from both sides of eq. (13). Then, employing the well-known result for the differentiation of implicit functions we have

$$\frac{dL_g}{dL} = -\frac{\partial\phi/\partial L}{\partial\phi/\partial L_g}, \quad (15)$$

where

$$\frac{\partial \phi}{\partial L} = r^2(L)\pi + \frac{dV_{\text{men}}}{dL} - \pi R^2 \left(1 + \frac{dh}{dL}\right)$$

and

$$\frac{\partial \phi}{\partial L_g} = -r^2(L_g)\pi + \pi R^2.$$

The actual value of L_g can only be determined by a numerical procedure. From eq. (13) we get

$$\frac{\int_0^L r^2 \pi dL + \frac{m_B}{\rho_B} + V_{\text{men}}}{\pi R^2} - (L + h) = \frac{\int_0^{L_g} r^2 dL}{R^2} - L_g, \tag{16}$$

where the left-hand side includes only known quantities.

While the entire crystal is submerged in B_2O_3, $m_g = 0$ and $dm_g/dL = 0$. In that case the counterpart of the volume balance in eq. (13) is of the form

$$\int_0^L r^2 \pi dL + V_B + V_{\text{men}} = \pi R^2 (L + h + \Delta), \tag{17}$$

where Δ is the distance of the tip of the crystal from the $B_2O_3(\ell)$ – gas interface. Rearranging eq. (17) yields

$$\frac{\int_0^L r^2 \pi dL + \frac{m_B}{\rho_B} + V_{\text{men}}}{\pi R^2} - (L + h) = \Delta. \tag{18}$$

Comparing eqs. (16) and (18) we observe that the left-hand sides are identical. As the crystal protrudes through the encapsulant, Δ changes from positive [eq. (18)] to negative [eq. (16)]. This provides an important clue in the computation of L_g. The numerical solution of eq. (16) for L_g starts when $\Delta = 0$.

2.2 Determination of the macroscopic growth rate, dL/dt

The macroscopic growth rate given in eq. (7) can be rewritten as

$$\frac{dL}{dt} = \frac{d\ell}{dL}\frac{dL}{dt} - \frac{dh}{dL}\frac{dL}{dt} + p. \tag{19}$$

Hence, by a rearrangement of eq. (19) dL/dt becomes

$$\frac{dL}{dt} = \frac{p}{1 - d\ell/dL + dh/dL}. \tag{20}$$

To eliminate the melt coordinate ℓ we use the relation for the conservation of melt [eq. (8)], which gives

$$\ell = \frac{m + \rho_\ell V_{\text{men}}}{\rho_\ell \pi R^2} = \frac{\pi \int_0^L \rho r^2 dL + \rho_\ell V_{\text{men}}}{\rho_\ell \pi R^2}. \tag{21}$$

Differentiating eq. (21) with respect to L yields

$$\frac{d\ell}{dL} = \frac{r^2}{kR^2} + \frac{dV_{\text{men}}/dL}{\pi R^2}. \tag{22}$$

Finally, introducing eq. (22) into eq. (20) gives the macroscopic growth rate in the form

$$\frac{dL}{dt} = \frac{p}{1 - \left(\frac{r^2}{kR^2} + \frac{dV_{\text{men}}}{dL} \Big/ \pi R^2\right) + \frac{dh}{dL}}. \tag{23}$$

2.3 Transformation of the crystal length to time coordinate

In general, r is known as a function of L. On the other hand the DWGS is recorded as a function of time. Therefore, a transformation from L to t is necessary in the analysis. From the continuity condition [eq. (6)] t can be expressed as

$$t = \frac{L + h(L) - \ell(L)}{p}. \tag{24}$$

Substituting eq. (21) into eq. (24) yields

$$t = \left(L + h - \frac{\int_0^L r^2 dL}{kR^2} - \frac{V_{\text{men}}}{\pi R^2}\right) \Big/ p. \tag{25}$$

2.4 Meniscus height and related properties

Mika and Uelhoff[11] have determined the meniscus shape and interface height, h, occurring during Czochralski growth by a numerical solution of the Euler-Laplace differential equation. Although, in principle, numerical results for the meniscus could be generated concurrently with the computation of the DWGS, here we prefer to rely on faster closed form solutions of the capillary equation. Fortunately, as shown by Mika and Uelhoff,[11] the analytical approximation of Tsivinskii[12] describes the exact values of h with excellent precision over a wide range of joining angles, α, and radii. We have verified that for $\alpha \lesssim -10°$ and $r \lesssim 0.5$ cm the error in using Tsivinskii's approximation is less than ~2 percent. Subsequent computer simulations have demonstrated that in practical situations, except when there is a very rapid

drop in radius, the stated limit on α is obeyed. The fact that for a short time after seeding r is less than 0.5 cm is of minor importance owing to the initial insensitivity of the DWGS to h.

Therefore, Tsivinskii's equations[12] for the interface height and shape will provide the basis of our DWGS analysis. In our notation Tsivinskii's equation for h is of the form

$$h = A[(1 - \sin\alpha + u^2)^{1/2} - u], \tag{26}$$

where

$$u = \frac{A\cos\alpha}{4r(L)}$$

and A is a constant. According to Egorov, Tsivinskii and Zatulovskii's modification for LEC growth of Tsivinskii's original work A is given by[13]

$$A = \sqrt{\frac{2\sigma}{(\rho_\ell - \rho_B)g}}. \tag{27}$$

The joining angle α is the sum of the growing angle, ϕ, and contact (wetting) angle, β (Fig. 1), i.e.,

$$\alpha = \phi + \beta. \tag{28}$$

In general, β is a constant, while the growing angle is a function of the derivative dr/dL according to[9]

$$\tan\phi = \frac{dr}{dL}, \qquad \phi = \tan^{-1}\frac{dr}{dL}. \tag{29}$$

Thus, h [eq. (26)] can be expressed in terms of r and dr/dL at the solid-liquid interface.

Consequently, the required first derivative of h, dh/dL, includes the second derivative d^2r/dL^2. This can be readily shown by the substitution of the combined eqs. (28) and (29) into eq. (26). Then, using standard trigonometric relations for angle-sums and inverse functions and differentiating the expression thus obtained with respect to L we find

$$\frac{dh}{dL} = \frac{A}{\left[1 + \left(\frac{dr}{dL}\right)^2\right]^{1/2}}\left[\frac{uv - \lambda}{(1 - \sin\alpha + u^2)^{1/2}} - v\right], \tag{30}$$

where

$$\lambda = \frac{\frac{1}{2}\frac{d^2r/dL^2}{1 + \left(\frac{dr}{dL}\right)^2}\left(\cos\beta - \frac{dr}{dL}\sin\beta\right)}$$

$$v = -\frac{A}{4r^2}\left[\frac{rd^2r/dL^2}{1+\left(\frac{dr}{dL}\right)^2}\left(\frac{dr}{dL}\cos\beta + \sin\beta\right)\right.$$

$$\left. + \frac{dr}{dL}\left(\cos\beta - \frac{dr}{dL}\sin\beta\right)\right].$$

Another derivative of interest in eq. (12) is $d\alpha/dL$. From eqs. (28) and (29) we have

$$\frac{d\alpha}{dL} = \frac{d(\tan^{-1}dr/dL + \beta)}{dL} = \frac{1}{1+(dr/dL)^2}\frac{d^2r}{dL^2}. \tag{31}$$

A property closely related to the interface height is the volume of the skirt-shaped meniscus, V_{men} (Fig. 1), and its axial derivative dV_{men}/dL. The quantity V_{men} can only be evaluated by a numerical technique. Egorov et al.[13] provide the x, y coordinates of the meniscus in the form of the integral

$$x = \int_h^y \frac{Q}{\sqrt{1-Q^2}}\,dy + r(L), \tag{32}$$

where

$$Q = \sin\alpha - \left(\frac{1}{A^2} + \frac{\cos\alpha}{2rh}\right)(y^2 - h^2).$$

Owing to axial symmetry summing up narrow segments of area $x^2\pi$ provides the volume of the meniscus as

$$V_{\text{men}} = \pi\delta \sum_{y_i=0}^{y_i=h-\delta} x^2(y_i), \tag{33}$$

where δ is the thickness of a segment.

Apart from performing numerical differentiation, no simple method exists for the evaluation of dV_{men}/dL. If the shape of the meniscus is that of a right cylinder, then V_{men} and dV_{men}/dL are given by

$$V_{\text{cyl}} = r^2\pi h$$

and

$$\frac{dV_{\text{cyl}}}{dL} = 2r\pi h\frac{dr}{dL} + r^2\pi\frac{dh}{dL}. \tag{34}$$

Simulations indicate that the numerical derivative dV_{men}/dL is closely approximated by

$$\frac{dV_{\text{men}}}{dL} \simeq \frac{V_{\text{men}}}{V_{\text{cyl}}}\frac{dV_{\text{cyl}}}{dL}. \tag{35}$$

III. RESULTS AND DISCUSSION

3.1 Computing methods

We have succeeded in reducing the theoretical determination of the DWGS to a differential equation in r, dr/dL and d^2r/dL^2. Therefore, if the shape of the crystal is given, the DWGS is calculable; conversely, the DWGS completely defines the radius of the crystal at any moment of interest. Here, we address ourselves to the first part of the problem, though the eventual objective is diameter control emphasizing the DWGS.

The program to evaluate the DWGS was written in HP Basic. A key feature in the efficient organization of the computations is the use of subroutines for dm_g/dL [eq. (14)], dL_g/dL [eq. (15)], dL/dt [eq. (23)], h [eq. (26)], dh/dL [eq. (30)], $d\alpha/dL$ [eq. (31)], V_{men} [eq. (33)], dV_{men}/dL [eq. (35)], as well as for $r(L)$ and its first and second derivatives.

Numerical integration was necessary to obtain V_{men} and the crystal volumes between O and L and O and L_g. It was found advantageous to evaluate the crystal volumes in the main routine because during the simulated growth of a crystal incrementing L in steps of 0.1 cm, the accumulating volume elements could be retained in memory.

As mentioned earlier, the quantity L_g is only required after the seed emerges from the $B_2O_3(\ell)$ encapsulant. Mathematically speaking, this occurs when the left-hand side of eq. (16) or (18) becomes negative. To determine L_g, at each increment of L the left-hand side of eq. (16) is evaluated. Then, a linear search is performed, substituting trial values of L_g into the right-hand side of eq. (16) in the range $L_g' - 0.2$ to $L_g' + 0.4$ cm in steps of 0.01 cm, where L_g' is the previous solution to eq. (16) at $L - 0.1$ cm. In case the 0.01-cm mesh around L_g' was too coarse to yield a solution, an option with 0.001-cm increments was available.

There are several mathematical tools available to describe the shape of the grown crystal, $r(L)$. From the actual cross section a large number of r, L coordinates can be generated in tabular form. Then, one obvious choice is to employ an interpretation scheme based on point-by-point tabular values of $r(L)$ in addition to numerical first and second derivatives. A more sophisticated alternative is to determine the Fourier coefficients of the crystal shape. However, we have learned by experience that the most efficient and satisfactory scheme to convert the tabular data into functional form is by using cubic spline regression.

A cubic spline function is a piecewise polynomial of degree three that joins adjacent polynomials in "knots." At the knots the functional values as well as the first and second derivatives are continuous. Ordinarily, a spline passes through all the points within the interval bounded by two knots. In contrast, in spline regression a cubic least-square fit for the same points is obtained. We have adapted, for the

present application, Wold's spline regression technique in terms of *B*-splines.[14]

Fortunately, the key features of the DWGS can be illuminated without invoking advanced data-fitting techniques. A judiciously chosen elementary transcendental function representing $r(L)$, which has n continuous derivatives, will be found suitable to illustrate the effect of various factors governing the course of the DWGS.

3.2 Major influences on the derivative weight-gain signal

3.2.1 Crystal shape

Typical LEC crystals, including GaAs, exhibit a pronounced "shoulder" as the radius rapidly expands from the seed. Boule-to-boule variation in the rate of approach to and radius of curvature of the shoulder is not uncommon. A mathematical description of the shoulder, in general, and a prototype crystal, in particular, is possible by means of the probability density function of the lognormal distribution.[15] Accordingly, we can write for a seed diameter of 0.6 cm

$$r(L) = C\left[\frac{1}{sL\sqrt{2\pi}}\exp -\frac{(\ln^2 L/L_m)}{2s^2}\right] + 0.3. \tag{36}$$

The median length, L_m, and the constant s are chosen such that the maximum r is 2.8 cm at $L = 2.2$ cm. From these conditions we have

$$L_m = 2.2\exp(s^2)$$

and a lengthy expression for C that is also only dependent on the standard deviation, s. Hence, the function $r(L)$ can be constructed if s is given.

In Figs. 2, 3, and 4 we present the crystal shape $r(L)$ for $s = 0.4$, 0.8, and 1.2, respectively. It can be seen that with decreasing s the radius of curvature at the maximum decreases (i.e., $|d^2r/dL^2|$ increases). Furthermore, it can be shown that the rate of approach to the shoulder (dr/dL) rapidly rises as s diminishes.

Substituting eq. (36) and its first and second derivatives into the DWGS [eq. (12)] and the subsidiary equations yields the signal and the crystal cross section as a function of time, both of which are shown in Figs. 2, 3, and 4. The required parametric values are listed in Table I. The results demonstrate that the DWGS is extremely sensitive to dr/dL and $|d^2r/dL^2|$. In fact, the steeper the rise in the shape, the sharper the peak in the DWGS and the larger its absolute magnitude.

Two other characteristic features of LEC pulling that are of crucial importance can also be observed in Figs. 2, 3, and 4. First, the maximum in DWGS precedes in time the maximum in shape by a few hundred seconds. This time lag we shall designate as the "precursor." The second property is the additional maximum in DWGS at a time when

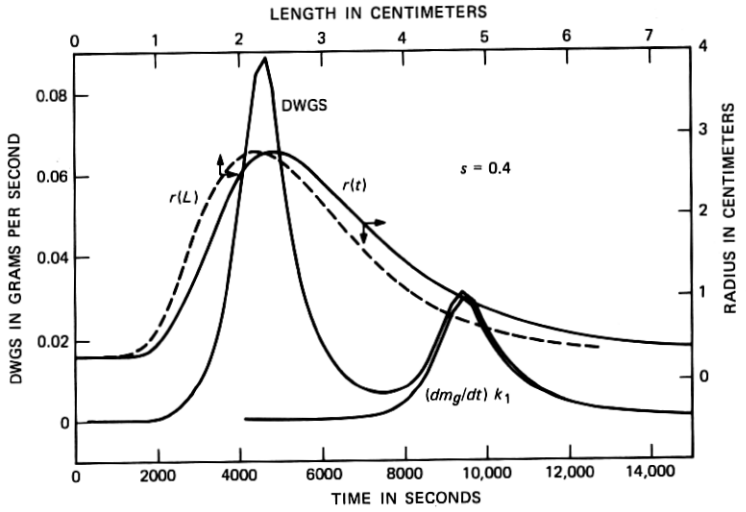

Fig. 2—The DWGS and crystal cross section as a function of time for LEC pulling. The shape versus length curve (– – –) is based on eq. (36), setting $s = 0.4$. The time derivative of the unencapsulated weight [dm_g/dt, eqs. (14) and (19)] is also shown.

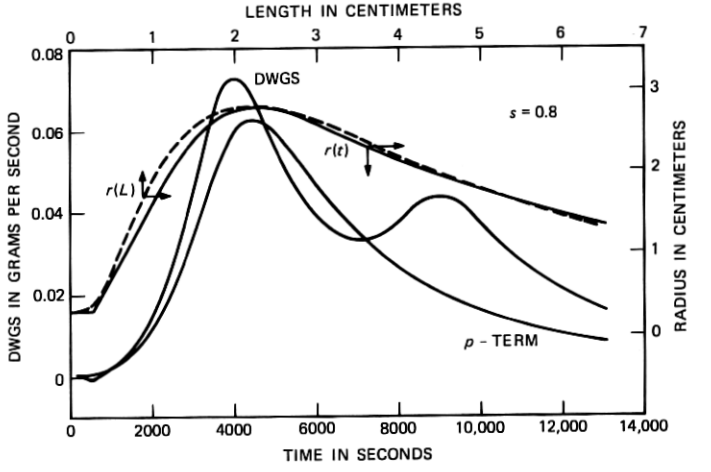

Fig. 3—The DWGS and crystal cross section as a function of time for LEC pulling. The shape versus length curve (– – –) is based on eq. (36), setting $s = 0.8$. The pull rate term in eq. (12)—the factor usually employed in conventional diameter control—is also shown.

the crystal's radius has already declined. We shall refer to this phenomenon as the "aftershock."

We have investigated the source of the precursor and aftershock. Simulations show that neither r nor its derivatives bears any responsibility. Examining the variation of the interface height with time (Fig.

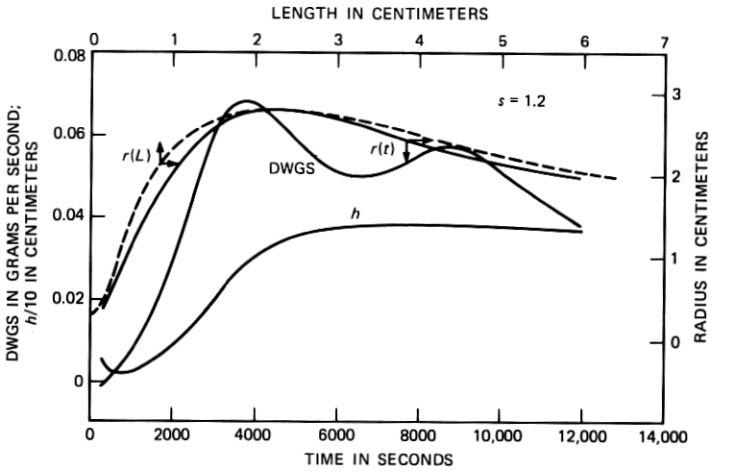

Fig. 4—The DWGS and crystal cross section as a function of time for LEC pulling. The shape versus length (- - -) curve is based on eq. (36), setting $s = 1.2$. The meniscus height [eq. (26)] is also shown.

Table I—Parameters for the calculation of the DWGS

Density of crystalline GaAs, d[g/cm^3]	5.17
Density of molten GaAs, d_ℓ[g/cm^3]	5.71
Density of $B_2O_3(\ell)$, d_B[g/cm^3]	1.55
Mass of $B_2O_3(\ell)$, m_B[g]	129.5
Pull rate, ρ[cm/s]	3.6×10^{-4}
Crucible radius, R[cm]	3.9
Wetting angle, β[deg]	15
Capillary constant, A[cm]	0.4
Surface tension, σ[dyne/cm]	333

4) we note that starting with a small but finite value at the seed, h saturates beyond the shoulder ($h \simeq 0.38$ cm).* Hence, no clue can be extracted from the form of h. Concentrating on the term including the pull rate in eq. (12), one concludes that this conventional description of the DWGS[3] holds quite well in the early phase of growth but departs from reality near the shoulder and beyond (Fig. 3). The maximum in the p term and the shoulder perfectly coincide and no secondary maximum appears.

If, however, one examines the derivative dm_g/dt [eqs. (14) and (23),

* The fact that at $t = 0$, $r \neq 0$, thus $h > 0$ is finite contradicts eq. (24). Therefore, to correct eq. (25) the residual time

$$t_0 = \left[h(L=0) - \frac{V_{\text{men}}(L=0)}{\pi R^2} \right] \Big/ p$$

is always subtracted from p.

Fig. (2)], it is found that this quantity rises from zero to a maximum value precisely at the time of the aftershock and that the magnitude of the DWGS in this regime is essentially dm_g/dt. In view of the fact that dm_g/dt is specifically associated with $B_2O_3(\ell)$ encapsulation, a reasonable hypothesis is that the aftershock is a consequence of the LEC technique.

3.2.2 Meniscus shape and liquid encapsulation

To isolate the factors leading to the precursor and aftershock we have evaluated the DWGS corresponding to the lognormal $r(L)$ [eq. (36), $s = 0.8$] in the absence of liquid encapsulation. In this case the major equations still hold provided ρ_B, V_B, m_B, m_g, and dm_g/dt are taken as zero. In Fig. 5 we present the DWGS with and without interposing a meniscus between the melt and the growing crystal. It is immediately obvious that in both instances the aftershock disappears from the DWGS. Moreover, if the meniscus is also removed, the precursor is missing, i.e., the times to reach the peak in DWGS and cross section exactly coincide. In fact by simultaneously eliminating $B_2O_3(\ell)$ and the meniscus from the growth system, only the contribution of the conventional pull rate term[3] is retained in eq. (12).

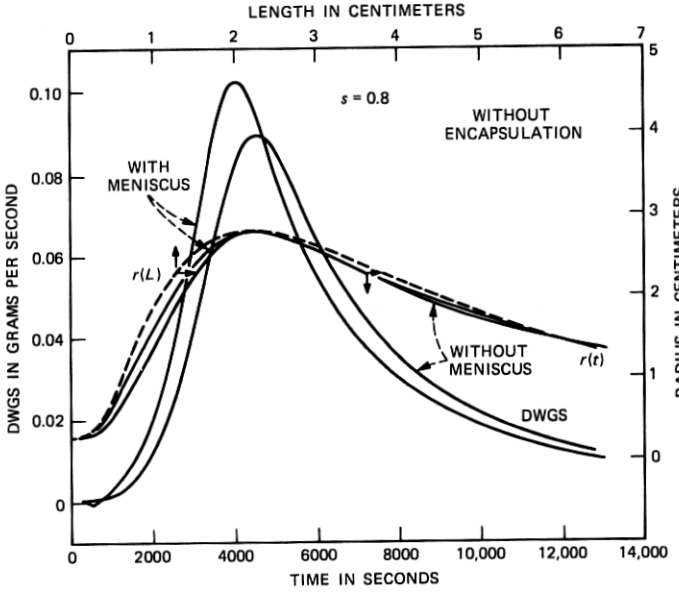

Fig. 5—The DWGS and crystal cross section as a function of time in normal Czochralski pulling without encapsulation. Curves with and without a meniscus present are given. The shape versus length curve (– – –) is based on eq. (36), setting $s = 0.8$. When the meniscus is absent, the pull rate term in eq. (12) exactly coincides with the curve shown.

Further confirmation of these effects is offered in Fig. 6. Here the calculation of the DWGS is repeated for LEC pulling without a meniscus. As we expected, though the precursor is missing the aftershock reappears. Apparently, up to and over the shoulder the DWGS is governed by the p term. Near the secondary maximum the derivative dm_g/dt becomes the dominant factor.

A more physical interpretation of the aftershock is possible by plotting the time-dependent radius, $r(L_g)$, of the crystal as it just protrudes through the $B_2O_3(\ell)$. In Fig. 6 we show both $r(L)$ and $r(L_g)$ as a function of time. Besides an expected displacement of the radius along the time axis one notes that the maximum in $r(L_g)$ occurs exactly at the time of the secondary maximum in DWGS. From these considerations a surprisingly simple explanation emerges. As more of the shoulder region becomes uncovered from the encapsulant, the DWGS registers the rapidly increasing true weight gain as opposed to the previously measured apparent (buoyancy-reduced) weight gain of the crystal. Hence, at the time of the maximum aftershock both the freshly grown layers at L, submerged in $B_2O_3(\ell)$, and the sizable exposed portions at L_g are detected.

The discovery of the precursor and the aftershock has a significant bearing on the diameter control of GaAs. The precursor is an early warning signal that predicts a maximum in radius a few hundred seconds before the actual event. In other words the DWGs is already

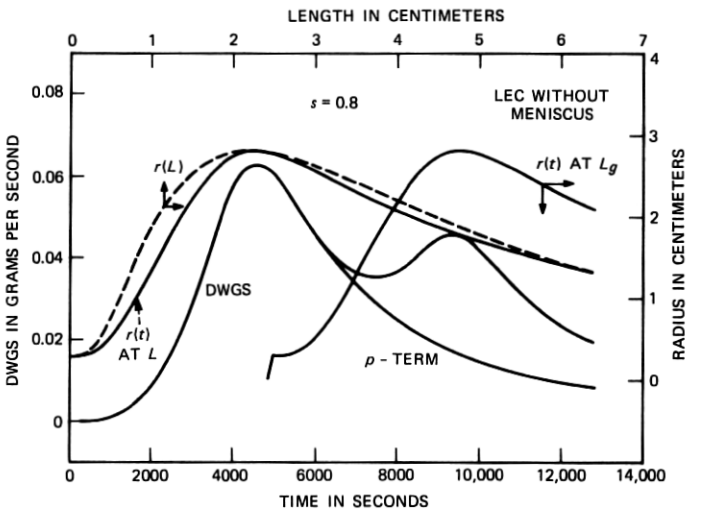

Fig. 6—The DWGS and crystal cross section as a function of time in LEC pulling, free of a meniscus. The radius is shown as a function of time at the solid-liquid interface, L, and at the top of the B_2O_3 layer, L_g. The pull rate term is also shown. The shape versus length curve (- - -) is based on eq. (36), setting $s = 0.8$.

dropping while the diameter is still increasing. Thus the controller has sufficient time to react to an unwanted change.

When the aftershock is observed there is a good chance that the controller misinterprets it as an unexpected gain in diameter and, if undesirable, will respond accordingly. Then, of course, a visible reduction in diameter will occur. By the time this is noticed, corrective action taken cannot restore the loss in diameter control. At best, beyond the shoulder a "sinusoidal" cross section with small amplitude results.

In view of these observations one cannot base the diameter control algorithm for GaAs on the customary p term[3] in eq. (12). To be sure, from the seed up to near the shoulder perhaps it suffices. However, for the bulk of the boule, control by means of such a traditional method is clearly inadequate.

3.3 Comparison with experiment

We have extracted the salient features of the DWGS arising during LEC pulling by the use of the lognormal probability function for the crystal's cross section. To compare the experimentally determined DWGS with the theoretical one the idealized crystal shape must be replaced by that of a GaAs boule grown by the LEC method under closely controlled conditions. Some of the growth parameters of interest for this specially prepared crystal are listed in Table I. The weight and length of the crystal are 523.3 grams and 6.6 cm, respectively.

The crystal coordinates (r versus L) can be derived from a two-dimensional projection employing a digitizer. Owing to the eccentricity of the actual ⟨100⟩ boule, a single view is insufficient. We have obtained planar projections with sharp contours by a photographic technique. The crystal was placed on the top of a light box, backlit, and photographed using a high-contrast film. Then, the procedure was repeated following a 90-degree rotation around the axis. In this manner, the two photos provided a total of four cross sections. Digitizing the shape in 0.5-mm intervals 133 pairs of (r, L) coordinates were collected for each of the four contours. At the shoulder the maximum error between the crystal and its projection is less than 0.5 percent. The computed mean weight is 528.6 g with a standard deviation of ±9.3 g, which should be compared with the measured weight of 523.3 g. Clearly, an excellent tabular description of the crystal's cross section has been accomplished. The data points for one of the four views are shown in Fig. 7.

The alternatives to represent the tabular data have been outlined earlier. In principle, because of close spacing, there would be no obstacle to a simple interpolation of the $r(L)$ values. However, as we illustrated in Fig. 7, using the numerical first and second derivatives may be problematic on account of noise. Indeed, when the DWGS was

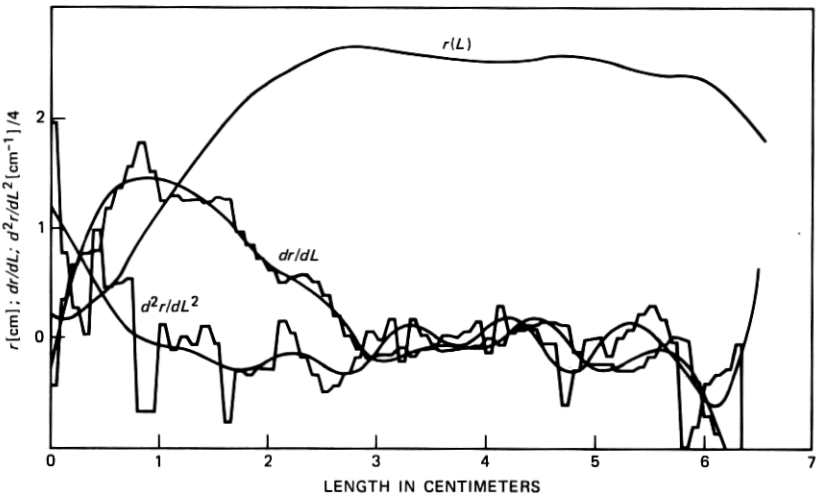

Fig. 7—One of the four experimental contours of a GaAs crystal and its cubic spline-regression representation (—). The cubic spline regression of the numerical first derivative dr/dL is also shown. In addition, the numerical second derivative d^2r/dL^2 is given, together with the quadratic expression derived from the cubic spline of dr/dL.

computed from the numerical derivatives severe discontinuities appeared in the results. This suggests that the steep "jumps" in d^2r/dL^2 seriously affect at some locations the shape and magnitude of the DWGS.

A different approach is the finite Fourier transform of the $r(L)$ points. However, owing to slow convergence a large number of terms is required. Eight terms were found to be sufficient to describe the seed and shoulder regions. Beyond the shoulder 18 terms were necessary to fit the data, albeit with concomitant high-frequency noise. Since the number of required terms was unpredictable and the computation inefficient, Fourier representation of the $r(L)$ data was abandoned. Nonetheless, the DWGS based on Fourier analysis provided a reasonable description of the measurements.

Cubic spline regression[14] has proven to be the most promising method to cast the tabular data on crystal cross sections into functional form. At the middle of the axis, the crystal was separated into two slightly overlapping domains and within each 12 equally spaced knots were positioned. The outstanding spline fit to one of the contours is given in Fig. 7. There are two avenues open to obtain the first derivative dr/dL. One is a simple differentiation of the shape's spline, which results in a continuous quadratic representation. Unfortunately, in this case the second derivative becomes a continuous network of connected straight lines (the third derivative is discontinuous) leading

to a jagged DWGS. A more fruitful approach is to fit the numerical first derivative itself by a cubic spline. Then, the noisy second derivative is described by a quadratic expression. In Fig. 7 we show the cubic spline fit to the numerical first derivative data as well as to the quadratic function passing through the numerical d^2r/dL^2. We note that a reasonably good description of the derivatives has been obtained by the spline regression technique. Therefore, all four contours were treated in a like manner.

Having thus established the shape and shape derivatives for an actual GaAs crystal, one can readily evaluate the corresponding DWGS by means of the analytical tools described earlier. Among the input parameters listed in Table I, all the densities were obtained from a recent critical evaluation of Jordan.[16] The selected contact angle (15 degrees) is consistent with theoretical and experimental findings on Ge and Si.[17,18,19] The capillary constant A and the surface tension, σ, are connected via eq. (27). Though the recommended value for A by Egorov et al. is 0.48 cm,[13] we have achieved a slightly better fit to the experimental DWGS using $A = 0.4$ cm, which is equivalent to $\sigma = 333$ dynes/cm. The surface tension of GaAs thus obtained is consistent with that for other III-V compounds (InP[20] and GaSb[21])Si and Ge.[22]

The gross appearance of the DWGS is not overly sensitive to a change in A. Nonetheless, a detailed examination reveals that the peak corresponding to the shoulder becomes higher and broader as A increases from 0.28 to 0.48 cm. With respect to the rest of the DWGS one can conclude that the peak-to-valley dynamic range diminishes as A drops. Among the effects of the other parameters, we have observed a rise in DWGS with an increase in p and a reduction of the time scale with a decrease in crucible radius.

In Fig. 8 we have reproduced the experimental derivative weight-gain signal as a function of time, as obtained on a carefully calibrated strip-chart recorder during the LEC growth of GaAs. The predicted DWGSs for the four contour lines as well as the time-dependent cross sections are also shown. Clearly the theoretical curves envelop the measured values, providing an excellent overall description.

The computed DWGSs exhibit both the early warning precursor and aftershock. In the inflection before the first peak we can discern the time when the seed first protrudes through the $B_2O_3(\ell)$. Since an actual crystal may possess additional cross-sectional bulges beside the shoulder, the secondary maximum in DWGS reflects both the memory of that earlier maximum in radius and the current expansion. To a small extent the DWGS is influenced by the input shape derivative function. For example, in the trough above the shoulder, a spline of the first derivative with many more knots would lead to a smoother transition to the next peak. Likewise, near the last peak, an improved

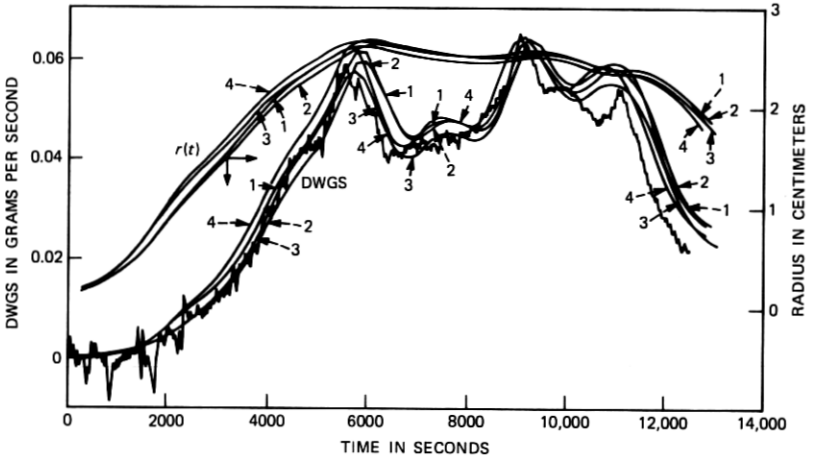

Fig. 8—DWGS (—) and crystal cross section as a function of time for four experimental contour lines of LEC-pulled GaAs. The measured DWGS was traced from the original strip-chart recording.

agreement with the experimental data is possible at the cost of a finer derivative spline. Near the bottom of the crystal the accord with the measured DWGS is more limited, perhaps on account of the increasingly negative turn in the joining angle α (between -20 and -40 degrees). Under those circumstances Tsivinskii's approximation for the meniscus properties becomes inaccurate.[11]

3.4 Prospects for diameter control

The excellent agreement between predicted and experimental DWGS strongly suggests that diameter control of GaAs by the derivative measurement is feasible. There are two approaches to diameter control implied by the modeling calculations. One is a real-time instantaneous determination of the radius during growth from the DWGS by solving the differential equation (12). Then, depending on whether r is increasing or decreasing from a preset limit, the RF input power is changed by a suitable amount.

The other method is the construction of an "ideal" crystal with appropriate tolerances on a drawing board. Taking into account the tolerances for this crystal, a band of DWGS can be evaluated as has been done for Fig. 8. Subsequently, the control of diameter is reduced to the problem of adjusting the power input in such a fashion that a template established by the band of DWGSs is followed.

IV. ACKNOWLEDGMENTS

We appreciate the continuing interest of J. W. Nielsen in this work and his critical reading of the manuscript. We thank L. J. Oster for the

expertly grown GaAs crystal and for his careful determination of the derivative weight-gain signal.

REFERENCES

1. D. T. J. Hurle, "Control of Diameter in Czochralski and Related Crystal Growth Techniques," J. Crystal Growth, *42,* No. 1 (December 1977), pp. 473–82.
2. R. E. Lorenzini, F. S. Nuff, and D. J. Blair, "An Overview of Si Crystal Growing Processes," Solid State Techn., *17,* No. 2 (February 1974), pp. 33–6.
3. A. J. Valentino and C. D. Brandle, "Diameter Control of Czochralski Grown Crystals," J. Crystal Growth, *26,* No. 1 (November 1974), pp. 1–5.
4. H. D. Pruett and S. Y. Lien, "X-ray Imaging Technique for Observing LEC Crystal Growth," J. Electrochem. Soc., *121,* No. 6 (June 1974), pp. 822–6.
5. H. J. A. van Dijk, C. M. G. Jochem, G. J. Scholl, and P. van der Werf, "Diameter Control of LEC Grown GaP Crystals," J. Crystal Growth, *21,* No. 3 (February 1974), pp. 310–12.
6. M. Cole, R. M. Ware, and M. A. Whitaker, paper presented at ECCG1, Zurich (1976).
7. P. Schmaker, A. Kramer, and W. Staehlin, paper presented at ECCG1, Zurich (1976).
8. R. M. Ware, private communication.
9. W. Bardsley, D. T. J. Hurle, and G. C. Joyce, "The Weighing Method of Automatic Czochralski Crystal Growth, Part I," J. Crystal Growth, *40,* No. 1 (September 1977), pp. 13–20.
10. W. Bardsley, D. T. J. Hurle, G. C. Joyce, and G. C. Wilson, "The Weighing Method of Automatic Czochralski Crystal Growth, Part II," J. Crystal Growth, *40,* No. 1 (September 1977), pp. 21–8.
11. K. Mika and W. Uelhoff, "Shape and Stability of Menisci in Czochralski Growth and Comparison with Analytical Approximations," J. Crystal Growth, *30,* No. 1 (August 1975), pp. 9–20.
12. S. V. Tsivinskii, Inzh. Fiz Zh., *5* (1962), p. 59.
13. L. P. Egorov, S. N. Tsivinskii, and L. M. Zatulovskii, "The Shape of the Melt Column in Growing a Crystal from Under a Flux Layer," Bull. Acad. Sci. USSR, Phys. Ser., *40,* No. 7 (1976), pp. 172–4.
14. S. Wold, "Spline Functions in Data Analysis," Technometrics, *16,* No. 1 (February 1974), pp. 1–11.
15. Y. L. Maksoudian, *Probability and Statistics with Applications,* Scranton, PA: International Text Book Co., 1969, pp. 123–4.
16. A. S. Jordan, "An Evaluation of the Thermal and Elastic Properties Affecting GaAs Crystal Growth," J. Crystal Growth, *49,* No. 4 (August 1980), pp. 631–42.
17. P. I. Antonov, "Capillary Phenomena in Crystal Growth" in *Growth of Crystals,* Vol. *6A,* ed., N. N. Sheftal, New York: Consultants Bureau, 1968.
18. T. Surek and B. Chalmers, "The Direction of Growth of a Crystal in Contact with Its Melt," J. Crystal Growth, *29,* No. 1 (May 1975), pp. 1–11.
19. T. Surek, "The Meniscus Angle in Ge Crystal Growth from the Melt," Scripta Met., *10,* No. 5 (May 1976), pp. 425–31.
20. A. S. Popov and L. Demberel, "Surface Tension of Molten Stoichiometric InP," Kristall Und Technik, *12,* No. 11 (1977), pp. 1167–70.
21. M. Ya. Dashevskii, G. V. Kukuladze, V. B. Lazarev, and M. S. Mirgalovskii, "Surface Effects in GaSb Melts," Inorg. Materials, *3,* No. 9 (September 1967), pp. 1360–66.
22. J. C. Phillips and J. A. VanVechten, "Macroscopic Model of Formation of Vacancies in Semiconductors," Phys. Rev. Lett., *30,* No. 6 (February 1973), pp. 220–3.